Effect of diffusion on acoustic deformation potential characterization through coherent acoustic phonon dynamics

Long Li, Feng He, Xu Zhao, Zhen Tong, and Liang Guo

Phys. Rev. B **106**, L060304 — Published 24 August 2022

DOI: 10.1103/PhysRevB.106.L060304

Effect of diffusion on acoustic deformation potential characterization through coherent acoustic phonon dynamics

Long Li[1, 5 ‡], Feng He[2 ‡], Xu Zhao[2], Zhen Tong[3, 6], and Liang Guo[1, 4, a)]

[1] Department of Mechanical and Energy Engineering, Southern University of Science and Technology, Shenzhen 518055, China.

[2] State Key Laboratory on Tunable Laser Technology, School of Electronics and Information Engineering, Harbin Institute of Technology Shenzhen, 518055, China

[3] Shenzhen JL Computational Science and Applied Research Institute, Shenzhen 518131, China

[4] Key Laboratory of Energy Conversion and Storage Technologies (Southern University of Science and Technology), Ministry of Education, Shenzhen 518055, China.

[5] School of Microelectronics, Shenzhen Institute of Information Technology, Shenzhen 518172, China.

[6] Beijing Computational Science Research Center, Beijing 100193, China

[‡] The authors contribute equally

[a)] Authors to whom correspondence should be addressed: guol3@sustech.edu.cn

ABSTRACT:

Ultrafast spectroscopy of coherent acoustic phonon (CAP) dynamics has recently been proposed as a method to characterize acoustic deformation potential (ADP), a key standard to quantify carrier-acoustic phonon coupling in semiconductors. In this Letter, we illustrate the importance of addressing the diffusion effect in ADP characterization by this method, using Ge as the demonstration system. It is found that the ADP mechanism and the thermoelastic effect have comparable contributions to CAP generation in Ge. Due to the different dependences on pump photon energies, the roles of these two mechanisms were assessed by varying pump wavelengths, based on which the ADP coupling constant of Ge was obtained. The analysis reveals that the carrier diffusion has a considerable impact on the shape of the CAP wave packet and must be processed cautiously for the ADP characterization for Ge.

Keywords: acoustic deformation potential, coherent acoustic phonon, ultrafast spectroscopy, carrier diffusion, germanium.

Interaction of carriers and acoustic phonons is the key to determine important physical properties such as thermal conductivity, carrier mobility, and emission linewidth. To quantify carrier-acoustic phonon coupling in semiconductors, acoustic deformation potential (ADP) was proposed, which describes electronic energy change by strain caused by long-wavelength longitudinal acoustic phonons [1, 2]. Although *ab initio* calculation can render the information about ADP [3, 4], it is elusive to extract the ADP parameters experimentally. Pressure-dependence measurements of optical properties can be applied to deduce the derivatives of energy gaps versus strain [5], but such methods may involve sample contamination by working mediums. Besides, the band-edge ADP parameters are related to carrier mobilities [1] and can be electrically measured. However, electrical measurement can only render absolute values of the ADP parameters and cannot distinguish carrier-acoustic phonon scattering from other scattering channels such as impurity scattering. Overall, there still lacks of a complete and accurate experimental technique for ADP characterization.

Ultrafast spectroscopy is powerful for studying coupling of electronic excitation with phonons [6-9]. One intriguing discovery by ultrafast spectroscopy is generation of coherent acoustic phonons (CAPs) [10, 11], which has been explored both fundamentally and technically [12-16]. Recently, experimental studies demonstrated that the dependence of CAP dynamics on excitation photon energies could be utilized to characterize the ADP of perovskites [17, 18]. This method relies on the fact that the photo-excited carriers impose a transient Coulomb force on the lattice through the ADP mechanism, contributing to CAP excitation. This non-invasive optical method provides an alternative way of ADP characterization, shows a great prospect for deepening our understanding of carrier-phonon coupling, and therefore deserves further exploration. Nevertheless, the influence of the carrier/heat diffusion, a key factor which can modify the CAP wave packet [12, 13], on the ADP characterization accuracy has not been explicitly discussed.

In this Letter, we reveal the importance of addressing the diffusion effect judiciously in ADP characterization by CAP dynamics, using Ge as the demonstration system. With a comprehensive study of the CAP dynamics for single-crystalline Ge, it is found that the ADP mechanism and the thermoelastic (TE) effect have comparable contributions to CAP generation in Ge. For Ge, the carrier diffusion has a significant impact on the CAP dynamics and hence the ADP characterization due to the faster carrier diffusion. Without carefully considering the carrier diffusion, the CAP-based

method can result in an absurdly irrational ADP coupling constant of Ge. This work paves the way for wider applications of the CAP-based analysis for study of electron-phonon coupling in semiconductors.

An intrinsic single-crystalline Ge (100) wafer with 0.5 mm thickness was used in this work. The output of an Yb: KGW femtosecond laser at 1030 nm with a repetition rate of 50 kHz (Pharos 10 W, Light Conversion) is split into two beams with a beamsplitter, as the pump and the probe. The pump and the probe go through two optical parametric amplifiers (Orpheus-N-2H and Orpheus-F, Light Conversion) for wavelength tuning. The probe is delayed versus the pump by a mechanical stage. The pump is modulated by a mechanical chopper at 500 Hz, and the transient reflectivity signal is processed by a lock-in amplifier (SR860, Stanford Research Systems) synchronized with the modulation signal. The pump spot is elliptical with the average spot diameters ($1/e^2$) 164, 128, and 187 μm at wavelengths 650, 680, and 800 nm, respectively. The corresponding pulse widths are 102.5, 141.2, and 118.2 fs measured by an autocorrelator (GECO, Light Conversion). The probe has spot diameters ($1/e^2$) in the range of 35 - 62 μm and pulse widths shorter than 200 fs.

Generation and detection of CAPs. The Ge sample was first tested with 800 nm pump and varied probe wavelengths from 625 to 920 nm. A typical transient reflectivity signal $\Delta R/R$ is presented in Fig. 1(a). After a sharp decrease and recovery signal associated with carrier excitation, a decaying oscillation signal (CAP signal) along with a slow recovery background appears. The inset of Fig. 1(a) illustrates generation and detection of the CAPs. The pump is absorbed near the sample surface due to the higher photon energy, 1.55 eV, than the band gap of Ge, 0.66 eV [19]. A CAP wave packet, i.e. a strain wave, is generated through both the electronic stress (related to ADP) and thermal expansion. Part of the strain wave travels into the sample while the rest towards the surface and is reflected, leading to a bipolar acoustic pulse [20]. The strain modulates the local dielectric constant, forming a moving optical interface. The probe is reflected at both the surface and this travelling interface. The oscillation signal is due to the interference of these two reflected beams. By removing the slowly varying background with a smoothing function (adjacent-averaging), the CAP signal can be obtained. Figure 1(b) presents the signals with the probe wavelengths 625, 730, and 920 nm, respectively. The solid lines were obtained through fitting with:

$$\frac{\Delta R}{R} = A\exp\left(-t/\tau\right)\cos\left(2\pi ft + \varphi\right) \quad (1)$$

where A, t, τ, f, and φ are the amplitude, the time delay, the decay time, the frequency, and the initial phase, respectively. As shown in Fig. 1(c), the extracted oscillation frequency f divided by twice the real part of the refractive index (n) [21] is inversely proportional to the probe wavelength λ_{pr}, consistent with the picture of Brillouin scattering [22], for which $f/(2n)=v/\lambda_{pr}$ with v being the longitudinal acoustic velocity [23]. The fitted slope is 4789.9±93.8 m/s, close to the reported sound velocity, 4870 m/s, perpendicular to the (100) plane of Ge [19]. This small discrepancy might come from the selection of the refractive index. Overall, this test justifies that the oscillation signal is caused by CAP propagation and guides the probe wavelength selection for ADP characterization.

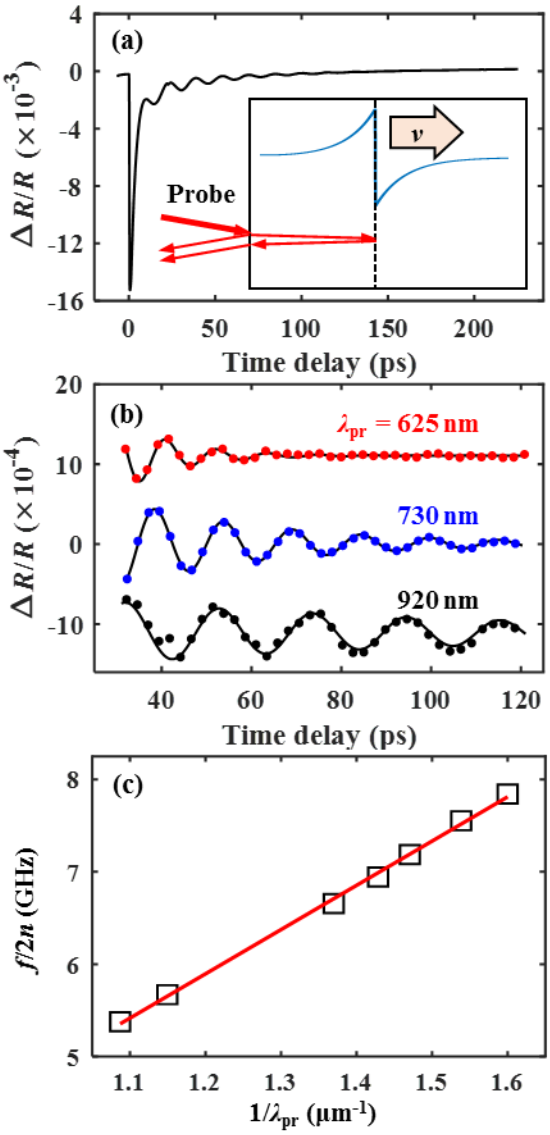

FIG. 1. (a) The transient reflectivity signal with 800 nm pump at the fluence of 0.5 mJ/cm^2 and 730 nm probe. The inset shows the schematic for CAP generation and detection: a CAP wave packet (a bipolar-shape strain wave, the blue curve) is excited by the pump and propagates into the sample at the longitudinal acoustic velocity; the strain alters the dielectric constant, forming a moving optical interface (the dashed line); the probe (the red arrow) is reflected partially at the surface and partially at the travelling interface; the interference of the two parts of reflection causes oscillation in the transient reflectivity signal. (b) The oscillation parts of the transient reflectivity signals probed at 625, 730, and 920 nm, with 800 nm pump at the fluence of 0.5 mJ/cm^2. The dots represent the experimental data and the solid lines are the fitting curves based on Eq. (1), which are offset for clarity. (c) The relationship between $f/(2n)$ and $1/\lambda_{pr}$. The squares represent $f/(2n)$ with f extracted experimentally. The error bars do not exceed the size of the symbols and are not shown. The red line represents the linear fitting function.

Pump fluence-dependent CAP-signal amplitude. We tuned the pump wavelength with the probe wavelength fixed at 740 nm (for which the oscillation signal is sufficiently strong and long-lasting). Figure 2(a) presents the CAP-induced oscillation signals with pump wavelengths 650, 680, and 800 nm and the fitting curves based on Eq. (1). The extracted oscillation amplitude A as a function of the pump fluence is shown in Figs. 2(b). The data points for 650 and 680 nm are shifted up for clarity. The solid lines in Fig. 2(b) represent the linear fitting of the first 4 amplitude values for each pump wavelength. Overall, the amplitude is larger at shorter pump wavelength and increases linearly with pump fluences when the fluence is below 0.63 mJ/cm^2. At higher fluence, the trend shows a sublinear relation. The first possible reason for this sublinear regime is screening of carrier-phonon coupling by high-concentration carriers [24, 25]. As previously reported experimentally, such screening occurs in Si when the carrier concentration exceeds 2×10^{20} cm^{-3} [24]. The sublinear trend here begins at 0.63 mJ/cm^2, corresponding to a carrier concentration of 1.15×10^{20} cm^{-3} for 680 nm, which is reasonable considering the similar electronic structures and non-polar features of Si and Ge [25]. Additionally, band filling, which may saturate pump absorption at high carrier concentrations, can also lead to such a sublinear trend [24]. Auger recombination at high carrier concentrations should lead to a superlinear trend and thus cannot explain our results [26]. A similar sublinear trend was observed in the CAP dynamics of MoS_2 [27]. The extracted frequency f and decay time τ as functions of the pump fluence are

shown and explained in S1 in Supplementary Material [28]. The decrease of the decay time at higher fluence may come from stronger absorption of the probe and enhanced carrier-phonon scattering due to increased free carrier concentrations, which is not the focus of this work since only the amplitude is used for extracting the ADP coupling constant. For ADP characterization, the pump fluence 0.315 mJ/cm^2 is selected to avoid the above-mentioned complicated effects.

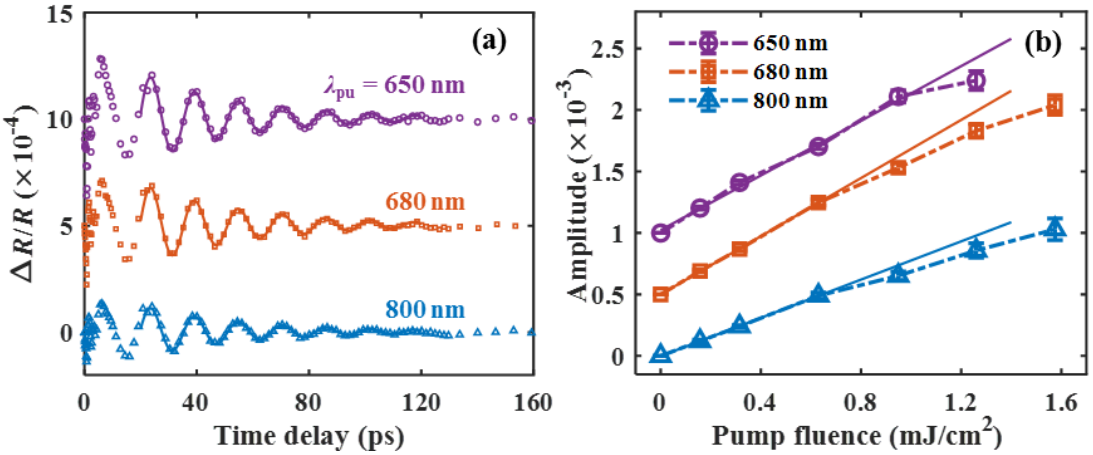

FIG. 2. (a) The CAP signals under pump wavelengths 650, 680, and 800 nm, at the fluence of 0.315 m*J*/cm^2, probed at 740 nm. The empty dots represent the experimental results and the solid curves represent the fittings with Eq. (1). (b) The oscillation amplitude as a function of the pump fluence from 0.157 to 1.57 mJ/cm^2. The solid lines represent the linear fitting of the first 4 values for each pump wavelength. The data points for 650 and 680 nm are shifted up by 4×10^{-3} and 2×10^{-3} in (a) and 1×10^{-3} and 0.5×10^{-3} in (b) for clarity.

Effect of the diffusion on ADP characterization. As a maturely developed semiconductor, the physical properties of Ge are well-known, including the ADP-related parameters. The reported ADP coupling constant ($\partial E_g/\partial\eta$ with E_g being the band gap and η indicating the strain) of Ge, -4 eV from *ab initio* calculation [3] and -3.75 eV from pressure dependent reflectance experiments [5] are reasonably close to each other. To further prove, we also performed *ab initio* calculation with density functional theory (DFT) to extract the band edge ADP parameters for the conduction and the valance bands, D_c and D_v (the derivative of the conduction band minimum and the valance band maximum versus the strain, D_c-D_v = $\partial E_g/\partial\eta$), from acoustic phonon scattering rates of Ge [36] (see S2 in Supplementary Material [28]). The result, $|D_c|+|D_v|$ = 4.1 eV (this calculation strategy, similar to electrical measurement [1], can only render the absolute values), also agrees well with the literature values [3, 5] (It implies that D_c and D_v have

opposite signs [1]). Thus, the ADP coupling constant of Ge around -4 eV can be safely used as a reference to test the accuracy of the CAP-based characterization method.

The electrostriction and the inverse piezoelectric effects are excluded for CAP generation because of the larger pump photon energies than the band gap and the centrosymmetric lattice for Ge [10], which are also advantages of taking Ge for demonstration. Consequently, two mechanisms, the ADP mechanism and the TE effect, contribute to CAP generation in Ge. The former results from the Coulomb interaction between the photo-excited carriers and the lattice through the ADP. The stress caused by the two mechanisms is described as [12, 37]

$$\sigma(z,t) = -B\frac{\partial E_g}{\partial P} N(z,t) - 3B\beta\Delta T(z,t) \tag{2}$$

where B is the bulk modulus, E_g is the band gap, P is the pressure, and β is the linear thermal expansion coefficient. $N(z, t)$ and $\Delta T(z, t)$ are the photo-excited carrier density and the lattice temperature rise dependent on the distance from the surface z and the time t. On the right-hand side of Eq. (2), the first term represents the contribution from the ADP mechanism, in which $-B\partial E_g/\partial P=\partial E_g/\partial \eta$ corresponds to the ADP coupling constant, while the second accounts for the TE effect. Considering the carrier and the thermal diffusion, N and ΔT can be evaluated by [12]

$$N(z,t) = \frac{\alpha_{pu}(1-R_{pu})F}{E_{pu}} \Theta_N(z,t) \tag{3}$$

$$\Delta T(z,t) = \frac{\alpha_{pu}(1-R_{pu})F(E_{pu}-E_g)}{E_{pu}\rho C} \Theta_T(z,t) \tag{4}$$

where α_{pu} is the absorption coefficient for the pump, R_{pu} is the reflectance, E_{pu} is the pump photon energy, F is the pump fluence, ρ is the density, and C is the heat capacity. The functions Θ_N and Θ_T can be expressed as following [12]

$$\Theta_N(z,t) = \int_{-\infty}^{\infty} (4\pi D_N t)^{-1/2} e^{-(z-z')^2/4D_N t} e^{-\alpha_{pu}|z'|} dz' \tag{5}$$

$$\Theta_T(z,t) = \int_{-\infty}^{\infty} (4\pi D_T t)^{-1/2} e^{-(z-z')^2/4D_T t} e^{-\alpha_{pu}|z'|} dz' \tag{6}$$

where D_N and D_T indicate the carrier and the thermal diffusion coefficients.

According to Eqs. (2) - (6), the stresses induced by the ADP mechanism and the TE effect depend differently on E_{pu} because N is related to the number of photons absorbed per unit volume while ΔT is related to the kinetic energy of the carriers. If the ADP mechanism dominates, the stress σ and thus the strain η (related to the oscillation

amplitude) should be proportional to $1/E_{pu}$ while if the TE effect dominates, they should scale with $(1-E_g/E_{pu})$. Therefore, the dependence of the CAP signal amplitude on E_{pu} contains the quantitative information about the relative magnitude of the two contributions. For pre-estimation, based on a previous experimental study [5], the ADP coupling constant of Ge is about -3.75 eV. The contribution ratios between the ADP mechanism and the TE effect, estimated by $(\partial E_g/\partial P)\rho C/[3\beta(E_{pu}-E_g)]$, for pump wavelengths 650, 680, and 800 nm are 3.72, 3.98, and 5.20, respectively (see S3 in Supplementary Material [28]). Therefore, in our experiments the two mechanisms should have comparable contributions to CAP generation, different from the cases for GaAs, Si, GaP, and GaN, for which the ADP mechanism dominates [13, 37, 38]. With the thermal properties known, the CAP amplitude variation versus E_{pu} can yield the ADP coupling constant.

The carrier and the thermal diffusion may affect the strain wave shape since they can change the spatial distribution of the stress and a dimensionless parameter, $D\alpha_{pu}/v$, can be used to quantify this impact [12], where D means the diffusion coefficient. The carrier diffusion coefficient can be calculated with the carrier mobility, which depends on the carrier concentration. With the pump fluence 0.315 mJ/cm^2, the photo-excited carrier concentrations for 650, 680, and 800 nm are 6.93×10^{19}, 5.76×10^{19}, and 3.69×10^{19} cm^{-3}, respectively. These are the estimated concentrations within the pump penetration depths of Ge, 78.3, 101.4, and 197.6 nm for the 3 pump wavelengths. With the carrier concentrations on the order of 1×10^{19} cm^{-3}, the electron and the hole mobilities are about 400 and 100 cm^2/Vs [39, 40]. The electron/hole diffusion coefficient $D_{e/h}$ can be obtained as 10.4 and 2.6 cm^2/s from the Einstein relations [41]. The ambipolar diffusion coefficient D_{am} was evaluated as 4.2 cm^2/s with $D_{am} = 2D_eD_h/(D_e+D_h)$ [13]. Note that the consideration of the carrier diffusion does not change the order of the carrier concentration, so our estimation is reasonable (see S4 in Supplementary Material [28]). The thermal diffusion coefficient of Ge is 0.36 cm^2/s [19], which is fixed in this work since it is well-determined. The α_{pu} values at 650, 680 and 800 nm are 1.23×10^5, 9.86×10^4, and 5.06×10^4 cm^{-1}, respectively [19]. Assuming α_{pu} as 1×10^5 cm^{-1}, the dimensionless parameters for the carrier and the thermal diffusion were estimated as 0.9 (obtained with D_{am}) and 0.07. According to the previously proposed criterion [12], the carrier diffusion has a notable impact on the strain wave shape and may also affect ADP characterization, while the thermal diffusion matters little for Ge.

Combining Eqs. (2) - (6) (see S3 in Supplementary Material [28]), the photo-induced stress can be calculated. The lattice displacement u and then the strain $\eta=\partial u/\partial z$ can be obtained by solving the following wave equation with the initial conditions $u(z, 0)=0$ and $\partial u(z, t)/\partial t|_{t=0}=0$, and the free boundary condition

$$\rho \frac{\partial^2 u(z,t)}{\partial t^2} = \frac{\partial \sigma(z,t)}{\partial z} \tag{7}$$

Figures 3(a) and 3(b) present the calculated strain spatial distributions at 25 and 120 ps with different assumed carrier diffusion coefficients (considering the uncertainty of the carrier diffusion coefficient with respect to the carrier concentration) and the fixed thermal diffusion coefficient. The ADP coupling constant was taken as -3.75 eV [5] temporarily. Clearly, the carrier diffusion significantly influences the strain wave shape by smearing the trailing side, consistent with the analysis based on the dimensionless parameter, and it must be considered for analyzing the CAP signal.

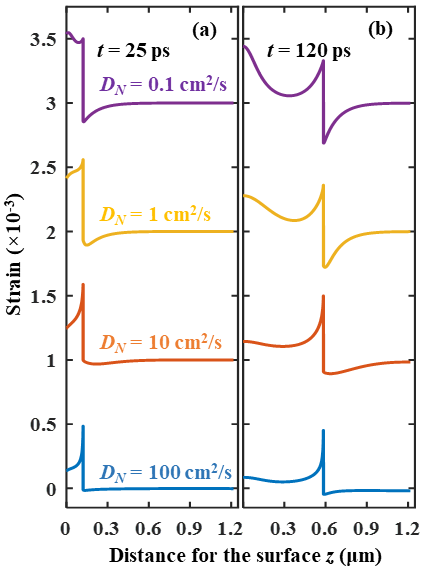

FIG. 3. The spatial distributions of the strain in Ge at (a) 25 ps and (b) 120 ps with carrier diffusion coefficients 0.1, 1, 10, and 100 cm^2/s. The curves are shifted vertically for clarity and the strain at the distance of 1.1 μm is zero for all the cases.

The carrier diffusion effect on the ADP characterization accuracy is investigated next, which may guide future work on carrier-acoustic phonon coupling. For a fixed probe, the relative change of the reflection coefficient r caused by the CAP-associated strain can be described by [37, 42]

$$\frac{\delta r(t)}{r_0} \propto \int_0^\infty \eta(z',t) e^{2ik_{pr}z'} dz' \tag{8}$$

where r_0 is the complex reflection coefficient for the probe without excitation, k_{pr} denotes the probe wave number in Ge, z' denotes the integrand variable, and t denotes the time delay. The oscillation part of the transient reflectivity signal can be further calculated by $\Delta R(t)/R=2\text{Real}[\delta r(t)/r_0]$ (see S5 in Supplementary Material for the deduction [28]) and Fig. 4(a) presents the calculated oscillation signals with the carrier and the thermal diffusion coefficients taken as 4.2 cm^2/s and 0.36 cm^2/s. The ADP coupling constant for these trial results was fixed as -3.75 eV [5]. The amplitudes of the calculated oscillation signals with different pump wavelengths were extracted with Eq. (1) and compared with the experimental results extracted from the CAP signals at the fluence of 0.315 mJ/cm^2 (Fig. 2(b)).

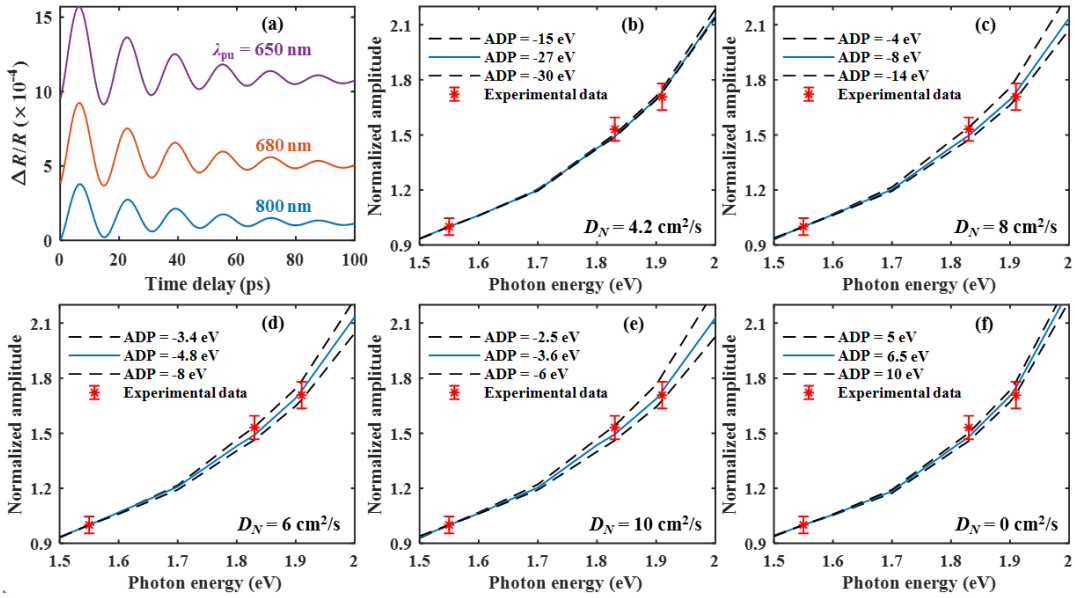

FIG. 4. (a) The calculated damping oscillation signals with pump wavelengths 650, 680, and 800 nm at the fluence of 0.315 mJ/cm^2. Extraction of the ADP coupling constant by fitting the experimental normalized amplitudes as functions of E_{pu} assuming different carrier diffusion coefficients (b) 4.2 cm^2/s, (c) 6 cm^2/s, (d) 8 cm^2/s, (e) 10 cm^2/s, and (f) 0 cm^2/s. The blue curves correspond to the best fitting while the black dashed curves illustrate exemplary deviating fitting by improper ADP coupling constants.

Since the carrier diffusion coefficient has a significant influence on the strain wave shape and the available value is diverse in literatures due to various carrier and impurity concentrations, the value of D_{am} (4.2 cm^2/s), and another three assumed values, 6, 8 and 10 cm^2/s, were chosen for the carrier diffusion coefficients to calculate the CAP signals. In addition, we also derived analytically the CAP signals without the carrier and the

thermal diffusion (see S6 in Supplementary Material [28]) for showing the unreasonable ADP characterization result with the carrier diffusion ignored. The curves, showing the relationship between the oscillation amplitude (normalized by the amplitude under 800 nm/1.55 eV excitation) and E_{pu}, can be calculated by adjusting the ADP coupling constant to fit the experimental trend. The best fitting curves with different carrier diffusion coefficients and without diffusion are presented in Figs. 4(b)-4(f). The best fitting values of the ADP coupling constants were as -27, -8, -4.8, -3.6, and 6.5 eV, for the carrier diffusion coefficients at 4.2, 6, 8, 10 cm^2/s, and neglecting the diffusion, respectively (see S7 in Supplementary Material [28] for the fitting details). With the diffusion effect ignored (Fig. 4(f)), there is even a change of the sign of the ADP coupling constant (6.5 eV versus the well-accepted value around -4 eV). The dramatic discrepancies among the extracted values testify that the diffusion effect must be considered carefully during the ADP characterization using the CAP-based method for Ge and other materials with fast carrier or thermal diffusion. The key of this method is to evaluate the dependence of CAP signal amplitudes on E_{pu}. Since large E_{pu} often corresponds to large absorption coefficients and short penetration depths, for which the diffusion effect becomes more significant, special attention should be paid to the fitting within the range of large excitation photon energies.

Compared with the reported ADP coupling constant values, -4 eV [3] and -3.75 eV [5], the obtained ADP coupling constant, -3.6 eV, with the carrier diffusion coefficient 10 cm^2/s is the closest, larger than the estimated ambipolar diffusion coefficient 4.2 cm^2/s. One reasonable explanation is that the cited mobilities are smaller than the actual mobilities in our experiments. In literatures [39, 40], the samples were heavily doped and the accompanied impurities can scatter the carriers and decrease the mobilities. While in this work, the carriers were excited optically and the photo-induced carrier mobilities may be several times larger than the literature values [36]. It is noteworthy that in CAP-based ADP characterization, pump with too large photon energies may induce multiple electronic transitions and complicate the ADP characterization especially for multi-valley band structures, the effect of which has not been studied to the best of our knowledge and is worth future research.

According to the theoretical derivation in two recent works [44, 45], there could be alternative strategies to obtain the ADP coupling constant based on the CAP dynamics. If the absolute value of $\Delta R/R$ and the Seraphin coefficient $\partial\varepsilon/\partial E$ (ε is the dielectric constant and E is the energy) can be accurately measured, then the ADP coupling

constant can be determined at just one combination of pump and probe photon energies [44]. However, measuring the absolute value of $\Delta R/R$ consistently requires careful adjustment of the laser parameters such as pulse widths and spot sizes, which is technically difficult. Also, measurement of ε spectrum usually involves fitting of ellipsometry data with many parameters, which depends on the familiarity with the band structure and is often challenging for novel materials. This is also the limitation of the method in the latter work [45], which relies on critical point energy analysis with ellipsometry. The method based on E_{pu} dependence analysis only needs to quantify the relative trend of $\Delta R/R$ versus E_{pu} instead of the absolute value and does not require the knowledge of ε, releasing some technical difficulties. As mentioned, there still lacks a perfect experimental technique for ADP characterization and all these available methods can be selected and cooperated to boost understanding of carrier-acoustic phonon coupling.

In summary, we have tested the recently proposed ADP characterization method based on CAPs with Ge as the demonstration system. It is found that the carrier diffusion must be taken into consideration in the analysis of the strain wave shape and the ADP characterization in order to render the reasonable ADP coupling constant, due to the larger carrier diffusion coefficient of Ge. Similar to the strain wave shape, when the dimensionless parameter $D\alpha_{pu}/v$ is close to or larger than 1, the diffusion effect needs to be carefully addressed. This could be a potential limitation of this method. Generally, thermal diffusion can be quantified by time-domain thermoreflectance, thermal transient grating, and so on [46, 47] while the carrier diffusion coefficient can be derived from the electrically measured carrier mobility by the Einstein relations or measured from transient spectroscopy [43]. In electrical measurement, doping is often necessary to ensure sufficient carrier density and thus defect scattering is inevitable, which also influences carrier motion. Since the CAP-based method is optical and involves no doping, we think measuring the carrier diffusion coefficient by transient spectroscopy could be a better choice to ensure ADP characterization accuracy.

This work is supported by the Guangdong Basic and Applied Basic Research Foundation (2019A1515010745, 2021A1515110606, 2021A1515011688), the University Consistent Support Program of Shenzhen Natural Science Foundation (20200925155828001), the National Natural Science Foundation of China (52176075, 51806094, 52106068), the Introduced Innovative R&D Team of Guangdong

(2017ZT07C062), and Shenzhen Science and Technology Program (KQTD20170810110250357).

L. L. and F. H. contributed equally to this work.

REFERENCES

[1] J. Bardeen and W. Shockley, Phys. Rev. **80**, 72 (1950).

[2] T. H. Liu, J. Zhou, B. Liao, D. J. Singh and G. Chen, Phys. Rev. B **95**, 075206 (2017).

[3] S. Wei and A. Zunger, Phys. Rev. B **60**, 5404-5411 (1999).

[4] C. Xia, J. Cui and Y. Chen, ACS Appl. Electron. Mater. **2**, 2745 (2020).

[5] R. Zallen and W. Paul, Phys. Rev. **155**, 703 (1967).

[6] J. Hohlfeld, S. S. Wellershoff, J. Gudde, U. Conrad, V. Jahnke, and E. Matthias, Chem. Phys. **251**, 237-258 (2000).

[7] A. K. Basak, H. Petek, K. Ishioka, E. M. Thatcher, and C. J. Stanton, Phys. Rev. B **91**, 125201 (2015).

[8] B. Liao, A. A. Maznev, K. A. Nelson, and G. Chen, Nat. Commun. **7**, 13174 (2016).

[9] S. Gerber, S. L. Yang, D. Zhu, H. Soifer, J. A. Sobota, S. Rebec, J. J. Lee, T. Jia, B. Moritz, C. Jia, A. Gauthier, Y. Li, D. Leuenberger, Y. Zhang, L. Chaix, W. Li, H. Yi, G. L. Dakovski, S. Song, J. M. Glownia, S. Nelson, K. W. Kim, Y. D. Chuang, Z. Hussain, R. G. Moore, T. P. Devereaux, W. S. Lee, P. S. Kirchmann, and Z. X. Shen, Science **357**, 71-75. (2017).

[10] P. Ruello and V. E. Gusev, Ultrasonics **56**, 21-35 (2015).

[11] A. Devos, Ultrasonics **56**, 90-97 (2015).

[12] C. Thomsen, H. T. Grahn, H. J. Maris, and J. Tauc, Phys. Rev. B **34**, 4129 (1986).

[13] O. B. Wright, B. Perrin, O. Matsuda, and V. E. Gusev, Phys. Rev. B **64**, 081202 (2001).

[14] A. Devos, J.-F. Robillard, R. Cote, and P. Emery, Phys. Rev. B **74**, 064114 (2006).

[15] K. Ishioka, A. Rustagi, A. Beyer, W. Stolz, K. Volz, U. Höfer, H. Petek, and C. J. Stanton, Appl. Phys. Lett. **111**, 062105 (2017).

[16] S. L. Cavera, P. Fernando, R. J. Smith, and C. Matt, Light Sci. Appl. **10**, 91 (2021).

[17] P. A. Mante, C. C. Stoumpos, M. G. Kanatzidis, and A. Yartsev, Nat. Commun. **8**, 14398 (2017).

[18] B. Wu, W. Ning, Q. Xu, M. Manjappa, M. Feng, S. Ye, J. Fu, S. Lie, T. Yin, F. Wang, T. W. Goh, P. C. Harikesh, Y. K. E. Tay, Z. X. Shen, F. Huang, R. Singh, G. Zhou, F. Gao, and T. C. Sum, Sci. Adv. **7**, eabd3160 (2021).

[19] M. S. Shur, *Handbook Series on Semiconductor Parameters*, (World Scientific, 1996).

[20] S. A. Akhmanov and V. E. Gusev, Sov. Phys. Usp. **35**, 153 (1992).

[21] T. N. Nunley, N. S. Fernando, N. Samarasingha, J. M. Moya, C. M. Nelson, A. A. Medina, and S. Zollner, J. Vac. Sci. Technol. B **34**, 061205 (2016).

[22] V. E. Gusev and P. Ruello, Appl. Phys. Rev. **5**, 031101 (2018).

[23] H.-N. Lin, R. J. Stoner, H. J. Maris, and J. Tauc, J. Appl. Phys. **69**, 3816 (1991).

[24] T. Sjodin, H. Petek, and H.-L. Dai, Phys. Rev. Lett. **81**, 5664 (1998).

[25] E. J. Yoffa, Phys. Rev. B **23**, 1909 (1981).

[26] E. S. K. Young, A. V. Akimov, R. P. Campion, A. J. Kent, and V. Gusev, Phys. Rev. B **86**, 155207 (2012).

[27] S. Ge, X. Liu, X. Qiao, Q. Wang, Z. Xu, J. Qiu, P.-H. Tan, J. Zhao, and D. Sun, Sci. Rep. **4**, 5722 (2014).

[28] See Supplemental Material for the details about the parameters for the calculation; the derivation from the strain to the transient reflectivity signal; the oscillation amplitude calculation without the carrier and the thermal diffusion; the extraction of the ADP coupling constant; the methodology and computational details of the *ab initio* calculation [29-35].

[29] D. E. Aspnes and A. A. Studna. Phys. Rev. B **27**, 985 (1983).

[30] N. Troullier and J. L. Martins, Phys. Rev. B **43**, 1993 (1991).

[31] J. P. Perdew, K. Burke, and M. Ernzerhof, Phys. Rev. Lett. **77**, 3865 (1996).

[32] S. Li, Z. Tong, and H. Bao, J. Appl. Phys. **126**, 025111 (2019).

[33] Z. Tong and H. Bao, Int. J. Heat Mass Transf. **117**, 972 (2018).

[34] Z. Tong, S. Li, X. Ruan, and H. Bao, Phys. Rev. B **100**, 144306 (2019).

[35] G. Nilsson and G. Nelin, Phys. Rev. B **6**, 3777 (1972).

[36] B. Liao, B. Qiu, J. Zhou, S. Huberman, K. Esfarjani, and G. Chen. Phys. Rev. Lett. **114**, 115901 (2015).

[37] K. Ishioka, A. Rustagi, U. Höfer, H. Petek, and C. J. Stanton, Phys. Rev. B **95**, 035205 (2017).

[38] S. Wu, P. Geiser, J. Jun, J. Karpinski, and R. Sobolewski, Phys. Rev. B **76**, 085210 (2007).

[39] D. L. Rode, Phys. Stat. Sol. (b) **53**, 245 (1972).

[40] K. Toko, R. Yoshimine, K. Moto, and T. Suemasu, Sci. Rep. **7**, 16981 (2017).

[41] C. Hu, *Modern Semiconductor Devices for Integrated Circuits*, (Pearson/Prentice Hall, 2010).

[42] O. Matsuda and O. B. Wright, J. Opt. Soc. Am. B **19**, 3028-3041 (2002).

[43] K. Chen, M. N. Yogeesh, Y. Huang, S. Zhang, F. He, X. Meng, S. Fang, N. Sheehan, T. H. Tao, S. R. Bank, J.-F. Lin, D. Akinwande, P. Sutter, T. Lai, and Y. Wang, Carbon **107**, 233-239 (2016).

[44] P. Jiang, X. Qian, and R. Yang, J. Appl. Phys. **124**, 161103 (2018).

[45] J. A. Johnson, A. A. Maznev, J. Cuffe, J. K. Eliason, A. J. Minnich, T. Kehoe, C. M. Sotomayor Torres, G. Chen, and K. A. Nelson, Phys. Rev. Lett. 110, 025901 (2013).

[46] A. Baydin, R. Gatamov, H. Krzyzanowska, C. J. Stanton, and N. Tolk, Phys. Rev. B **99**, 165202 (2019).

[47] C. Emminger, S. Espinoza, S. Richter, M. Rebarz, O. Herrfurth, M. Zahradník, R. Schmidt-Grund, J. Andreasson, and S. Zollner, Phys. Status Solidi RRL **16**, 2200058 (2022).